Particle-size dependence of orbital order-disorder transition in $LaMnO_3$

Nandini Das, Parthasarathi Mondal, and Dipten Bhattacharya*
Electroceramics Division, Central Glass and Ceramic Research Institute, Calcutta 700 032, India
(Received 21 November 2005; revised manuscript received 23 May 2006; published 12 July 2006)

The latent heat (L) associated with the orbital order-disorder transition at T_{JT} is found to depend significantly on the average particle size (d) of $LaMnO_3$. It rises slowly with the decrease in d down to ~100 nm and then jumps by more than an order of magnitude in between $d \sim 100$ nm and ~30 nm. Finally, L falls sharply to zero at a critical particle size $d_c \approx 19$ nm. The transition temperature T_{JT} also exhibits an almost similar trend of variation with the particle size, near $d \sim 30$ nm and below, even though the extent of variation is relatively small. The zero-field-cooled (ZFC) and field-cooled (FC) magnetization versus temperature study over a temperature range 10–300 K reveals that the antiferromagnetic transition temperature decreases with d while the temperature range, over which the ZFC and FC data diverge, increases with the drop in d. The FC magnetization also is found to increase sharply with the drop in particle size. A conjecture of nonmonotonic variation in orbital domain structure with decrease in particle size—from smaller domains with large number of boundaries to larger domains with small number of boundaries due to lesser lattice defects and, finally, down to even finer domain structures with higher degree of metastability—along with increase in surface area in core-shell structure, could possibly rationalize the observed L versus d and T_{JT} versus d patterns. Transmission electron microscopy data provide evidence for presence of core-shell structure as well as for increase in lattice defects in finer particles.

DOI: 10.1103/PhysRevB.74.014410 PACS number(s): 75.50.Tt, 71.70.Ej, 64.70.Nd

The orbital physics assumes significance in strongly correlated electron systems[1] such as perovskite manganites or high-T_c superconductors not only because understanding the orbital physics provides vital clues to phenomena such as metal-insulator transition, superconductivity, colossal magnetoresistance, phase separation, interplay among orders in charge, spin, orbital degrees of freedom, etc. but also because of possible future applications of orbital electronics[2] in many areas of microelectronics. Recent works have shown how different orbital phases—solid, liquid, glass, liquid crystal, etc.—develop across a whole range of doped and undoped manganites.[3] Study of orbital order-disorder transition from both thermodynamics and kinetics points of view helps in ascertaining the nature of the orbital phases. Local structural studies namely, resonant x-ray scattering (RXS)[4] or coherent x-ray beam scattering[5] provide information about the orbital domain structure and its variation as a function of overall lattice distortion and charge carrier doping. It seems that through all these studies a comprehensive picture of orbital phases and their role in governing a range of distinct phenomena observed in strongly correlated electron systems is emerging.

It is interesting, in this context, to study the orbital order-disorder transition in confined geometries, e.g., in nanostructured systems. Nanostructured systems offer unique properties such as improved magnetization, quantum effects, improved mechanical property, etc.[6] By proper tuning of the particle size, it is possible to optimize the desired property—electrical, magnetic, optical, thermal, mechanical, etc. The phase transition characteristics also undergo drastic changes with the decrease in particle size down to less than 100 nm.[7] Sophisticated techniques such as ultrasensitive nanocalorimetry,[8] scanning tunneling microscopy together with perturbed angular correlation,[9] laser irradiation coupled with local calorimetry,[10] etc. have been used in order to study the melting phenomena in nanoparticles of metals. It has been observed that both the melting point (T_m) as well as the latent heat (L) depress as inverse of atom cluster radius (r) down to a cluster size of ~2 nm.[8–11] The phenomenon of melting follows either homogeneous melting[12] or liquid-shell melting[13] or nucleation and growth kinetics model.[14] The depression in T_m or L results from an increased surface area where atoms are rather loosely bound.

The study of orbital order-disorder transition in nanostructured $LaMnO_3$ assumes significance in the context of use of such nanostructured systems in microelectronics applications. It is also important in the context of understanding the variation in orbital domain structure as a function of particle size and thereby variation in spin structure. In this paper, we report results of orbital order-disorder transition studied by conventional global calorimetry in a series of nanostructured $LaMnO_3$ systems with different particle sizes. The latent heat (L) associated with the transition is found to follow a nonmonotonic pattern with the particle size d. The transition temperature (T_{JT}) is also found to follow nonmonotonic pattern. While the rise in L is more than an order of magnitude near $d \sim 30$ nm, the T_{JT} is found to have first dropped by more than ~10% with the drop in particle size and then exhibits a rise by a few degrees near $d \sim 30$ nm before finally decreasing by nearly ~30% with further decrease in particle size down to the critical size $d_c \approx 19$ nm. The latent heat (L) also drops precipitously within this particle size range. In order to rationalize the observation, we conjecture a variation in orbital domain structure as a function of particle size together with increase in surface area in core-shell structure of particles. The transmission electron microscopy (TEM) results provide information regarding core-shell structure and lattice defects as a function of particle size.

The nanocrystalline $LaMnO_3$ particles have been prepared by various techniques. For this work we have primarily resorted to bottom-up approaches[15] such as the preparation of

fine particles by using microemulsion[16] or precipitation from a solution under ultrasonic vibration.[17] These techniques have produced phase pure fine particles. In the case of microemulsion technique, a solution is prepared by mixing aqueous solutions of $La(NO_3)_3$ and Mn-acetate in 1:1 concentration ratio along with cetyltrimethyl-ammonium bromide (CTAB) as surfactant, *n*-butanol, and *n*-octane. The aqueous metal nitrate/acetate solution together with CTAB forms the microemulsion within *n*-octane. The *n*-butanol is added as a cosurfactant. Another emulsion having oxalic acid, CTAB, *n*-butanol, and *n*-octane is prepared. In this case, aqueous solution of oxalic acid together with CTAB forms the microemulsion within *n*-octane. This emulsion is added to the previous one under constant stirring. Each emulsion droplet acts as a nanoreactor. The emulsion droplets from the added solution coalesce with those in the earlier one and facilitate the precipitation reaction within the droplets whose size is restricted by the surfactant. The size of the droplets can be varied by changing the concentration of the surfactant which, in turn, gives rise to particles of different sizes. In the case of microemulsion technique, the concentration of the surfactant is increased from 8.5 to 9 mM/liter for reducing the particle size down to 20 nm. The precipitate, thus obtained from the resultant mixture, was centrifuged and washed with acetone and alcohol mixture. Finally, the powder was dried under vacuum at ~50 °C. In the case of sonochemical technique, aqueous solutions of lanthanum nitrate and manganese acetate were mixed and sonicated by using Ti horn (20 kHz, 1500 W, Vibracell, USA) for 2 h at room temperature. A small amount of decalin is added for efficient power transfer. To reduce agglomeration, sodium dodecyl sulphate (SDS) surfactant was added under sonication. Here too, the concentration of the surfactant is varied from 0.85 to 1 mM/liter for controlling the particle size. Oxalic acid is also added during sonication. Sonication is continued until precipitation is complete. Finally, the precipitate was collected, washed with alcohol and acetone and dried under vacuum at ~40 °C.

The powders prepared by both the techniques were subject to heat treatment under different temperatures for different time span. The temperature was varied between 700 and 800 °C while the time was varied between 4 and 6 h. The controlled variation in surfactant concentration as well as heat treatment time and temperature helps in preparing particles of different sizes. These parameters have been optimized in order to prepare powders with requisite particle size. The x-ray diffraction (XRD) patterns exhibit crystalline perovskite orthorhombic phase with *Pbnm* space group. A representative XRD pattern is shown in Fig. 1(a). In Fig. 1(b) we show representative high angle x-ray lines. From such line broadening one can normally calculate the average crystallite size (d) by using the Debye-Scherrer model. The Debye-Scherrer model can be written as $d=0.9\lambda/\beta_d \cos\theta$, where $\lambda=1.54056$ Å for the CuKα line, β_d is the full width at half maximum of an x-ray diffraction peak, and θ is the corresponding Bragg angle. The lattice strain (ε), on the other hand, as a function of particle size can be calculated by using the Wilson formula $\varepsilon=\beta_\varepsilon/4\tan\theta$ where β_ε describes the structural broadening, which is the difference in integral x-ray peak profile width between the sample and a standard

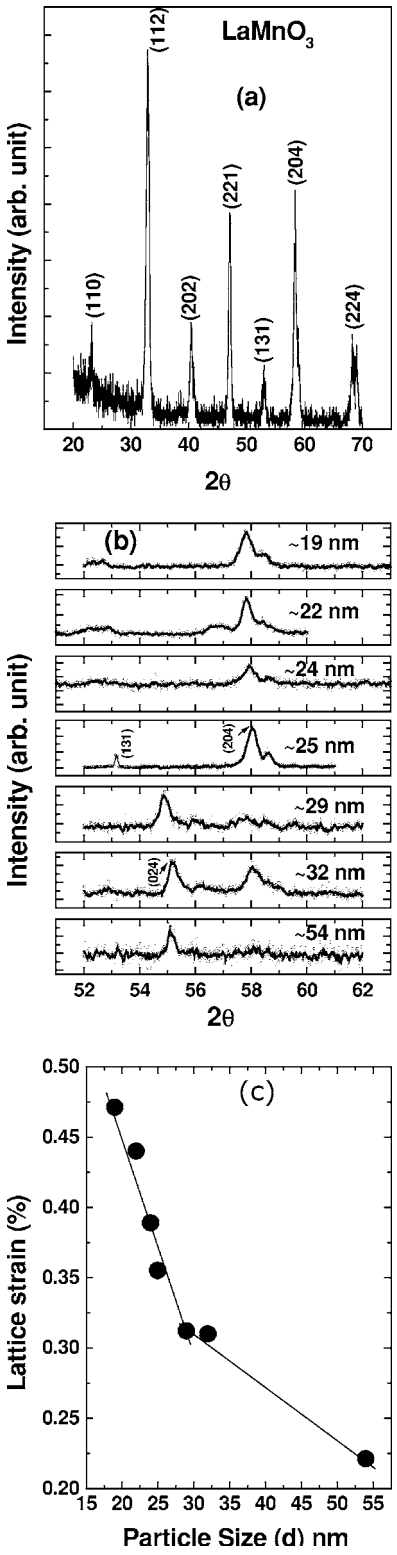

FIG. 1. (a) Typical room temperature X-ray diffraction pattern of the nanoparticles of $LaMnO_3$. The average crystallite size corresponding to this pattern is ~25 nm. (b) Representative high angle x-ray peaks blown up. The full width at half maximum (FWHM) is used for calculation of the crystallite size. (c) The lattice strain vs particle size (d) plot. The lattice strain appears to have increased at a faster rate below $d\sim30$ nm. The solid lines are guides to the eye.

(silicon) and is given by $\beta_{\varepsilon} = \sqrt{\beta^2_{\varepsilon.\mathrm{obs}} - \beta^2_{\mathrm{std}}}$. Silicon standard is used as it has a large crystallite size. However, since the actual x-ray peak broadening in the present case is taking place due to both the decrease in particle size and increase in lattice strain, we followed the Williamson-Hall approach to calculate the particle size (d) and the lattice strain (ε). In this approach, the experimental x-ray peak broadening (β_{exp}) is given by $\beta_{\mathrm{exp}} = 0.9\lambda/d \times \cos\theta + 4\varepsilon \sin\theta/\cos\theta$. By plotting $\beta_{\mathrm{exp}} \cos\theta$ as a function of $4 \sin\theta$ for several x-ray diffraction peaks, we obtained a straight line. This linearity shows that for our case the Williamson-Hall approach is applicable. The slope of the straight line gives the lattice strain (ε) while the crystallite size (d) is calculated from the intercept of the straight line with the vertical axis. The lattice strain is found to be compressive and varying between 0.22% and 0.48% with higher strain for finer particles [Fig. 1(c)]. The lattice strain appears to have increased at a faster rate below $d \sim 30$ nm.

In Fig. 2, we show the representative TEM photographs of the nanoparticle assemblies. Using an image analyzer, we determined the average particle size as well as the histogram of the particle size distribution. The average particle size is found to vary between 20 and 100 nm (aspect ratio 1.25–1.27). While presenting our data on nanoscale $LaMnO_3$, we use the average particle size estimated from the TEM study. We notice a bit of difference between the crystallite size estimated from XRD peak profile analysis and the particle size estimated from TEM study. This difference is due to the presence of lattice strain which influences the XRD peak profile. The core-shell structure of the particles can be clearly observed in TEM photographs of the finer systems. The high resolution TEM (HRTEM) picture helps in finding out the average lattice plane spacing. It varies between 0.2 and 0.4 nm. One interesting observation is the variation in lattice defect structure as a function of particle size. In finer particles, one observes defect lines and different facets in lattice structure [Fig. 2(b)] while in relatively coarser particles one observes rather defect-free lattice [Fig. 2(a)]. We have measured the Brunauer-Emmett-Teller (BET) specific surface area of the powder as well. It is found to vary between 16 and 20 m^2/gm. Poor surface area possibly results from agglomeration of the nanoparticles. All these data are consistent and, therefore, the quality as well as the average particle size of the powders appears to be well defined. The Mn^{4+} concentration is measured by chemical analysis (redox titration) and is found to be varying between 2 and 5%.

We have studied the orbital order-disorder transition by global calorimetry. In Fig. 3, we show differential scanning calorimetric (DSC) and differential thermal analysis (DTA) thermograms for a few samples having different particle sizes. Quite obviously, the phase transition peak position and area vary with the particle size. We have evaluated the latent heat by subtracting the background and calculating the peak area. We have also studied the low-field magnetic properties of the samples. The zero-field cooled (ZFC) and field-cooled (FC) magnetization versus temperature measurements have been carried out across a temperature range 10–300 K under a field ~100 Oe. The variation in magnetization with temperature for a few representative samples is shown in Fig. 4. It is found that the antiferromagnetic transition temperature

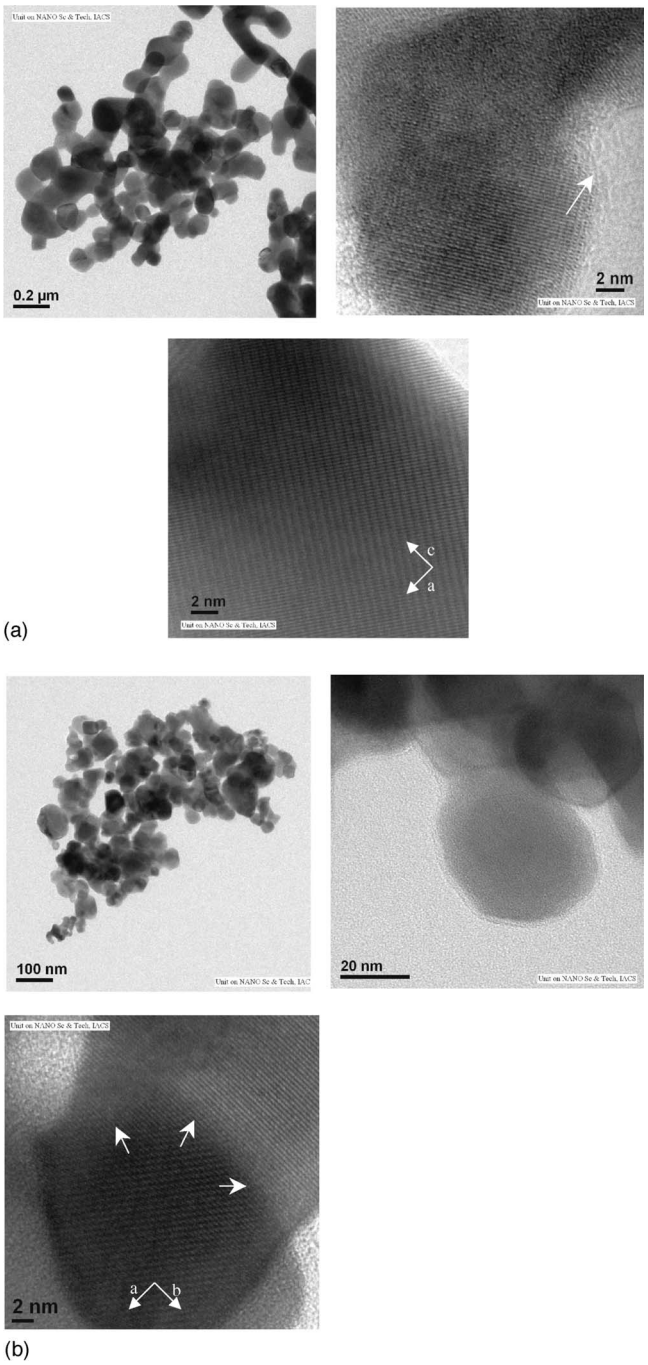

FIG. 2. (a) TEM and HRTEM photographs of the assembly of particles and lattice fringes within an isolated particle, respectively. The average particle size is found to be ~32 nm. The lattice planes appear to be defect free over a large region. The core-shell structure of the particles can be observed with shell thickness estimated to be ~5 nm. Arrow points to the shell region. (b) TEM and HRTEM photographs of the assembly of nanoscale particles and lattice fringes within an isolated particle, respectively. The average particle size is estimated to be ~20 nm. The lattice fringes appear to have changed the orientation across the defect line. The defect lines are evident and marked by arrows. The shell thickness is large and is estimated to be ~8 nm. Arrows point to a defect line.

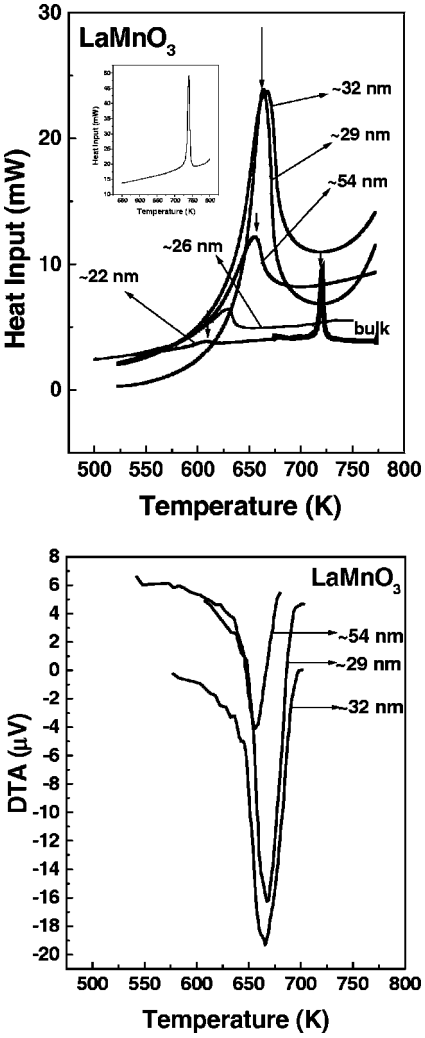

FIG. 3. DSC (top) and DTA (bottom) thermograms for few of the $LaMnO_3$ systems with different particle sizes are shown. Top inset: DSC thermogram for the $LaMnO_3$ single crystal is shown. The rate of heating was 10 °C/min.

(T_N) decreases systematically with the particle size d. On the other hand, the temperature range over which the ZFC and FC data diverge (ΔT) appears to increase with the decrease in particle size. For instance, for ~19 nm particle size, ΔT is ~255 K whereas for ~54 nm it is ~215 K. This implies increase in metastability. The FC magnetization increases with the decrease in particle size, which could be due to increase in surface magnetization. The variation of latent heat (L), T_{JT}, and T_N with the average particle size is shown in Fig. 5. The calorimetric study has been repeated several times on a particular sample as well as on freshly prepared samples in order to verify the reproducibility of the data. In all these measurements, less than 10% variation in L and less than ~2% variation in T_{JT} could be observed. The heating and cooling cycle data depict small amount of "thermal history" effect in peak position. The peak position differs in heating and cooling cycle by less than 2 K. These are the central results of this paper. For the sake of comparison, we have included the data corresponding to bulk polycrystalline as well as single-crystal $LaMnO_3$ samples. Good quality

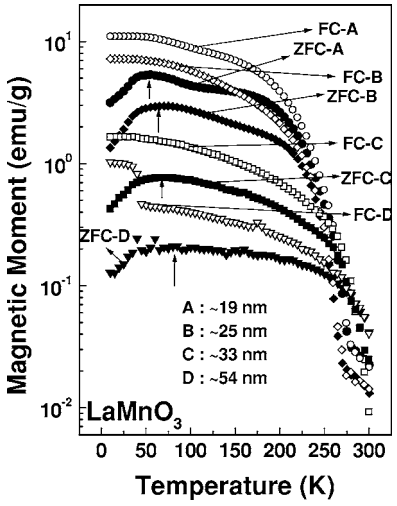

FIG. 4. Zero-field cooled (ZFC) and field-cooled (FC) magnetization vs temperature patterns for few of the nanocrystalline $LaMnO_3$ samples. The measurement has been carried out under an applied magnetic field 100 Oe.

single-crystal has been prepared by traveling solvent zone technique.

It is interesting to note that L is varying significantly with d. It rises by more than an order of magnitude with the decrease in d down to ~30 nm and then drops sharply to zero at a critical particle size $d_c \sim 19$ nm. This pattern apparently resembles the one of coercivity (H_c) versus d observed in nanocrystalline ferromagnetic systems.[18] The transition temperature T_{JT} also exhibits similar pattern, even though the rise is rather small. Such nonmonotonicity in L versus d and T_{JT} versus d patterns is a significant departure from those commonly observed in melting in nanoscale.[8–11] This result shows that one can improve the enthalpy change or latent

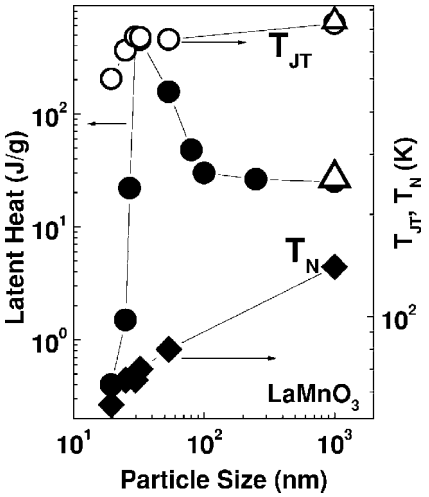

FIG. 5. The latent heat associated with orbital order-disorder transition vs average particle size in pure $LaMnO_3$. The variation of T_{JT} and T_N with the average particle size is also shown. The data corresponding to ~1 μm particle size represent those of bulk sample and single crystal. The data corresponding to the single crystal are marked by open up-triangle symbols ($T_{JT} \sim 740$ K, $L \sim 30$ J/g).

heat in $LaMnO_3$ around the orbital order-disorder transition point by resorting to nanoscale system. It also provides the limit of the particle size within which one is expected to observe such improvement. Such improved latent heat, if observed under electric or magnetic field or under pressure, can be utilized in different sensor applications.

It may also be noted, in this context, that normally both melting point as well as latent heat of melting are found to decrease systematically with d.[11] Here, even though the latent heat of orbital order-disorder transition is found to rise by more than an order of magnitude, the rise in transition temperature T_{JT} is small and is certainly not higher than that observed in bulk or single-crystal sample. Therefore, it appears that a rise in latent heat of transition is not always associated with concomitant rise in transition temperature. The patterns of L versus d and T_{JT} versus d can be understood, at least, *qualitatively* by resorting to the concept of orbital domain structure.

It seems that the overall orbital domain volume determines the latent heat. In a continuum, the latent heat would have followed a monotonic pattern of decrease with the decrease in particle size. The *nonmonotonicity* observed in the present case points out relevance of the discrete domains within a particle. The particle size alone does not determine the overall latent heat of transition at T_{JT}. In bulk $LaMnO_3$, the particles (or grains) are multidomain in nature. They contain both domain and domain boundaries. The domain boundaries are disordered and, therefore, do not undergo a first-order transition at T_{JT}. The net orbital domain volume is relatively small in bulk systems. As the particle size decreases, we reach essentially a cleaner, i.e., defect-free system which, in turn, leads to a sharp rise in domain volume with fewer domain boundaries. Of course, a direct observation of variation in orbital domain size as a function of particle size would have supported or discarded this conjecture. That experiment is beyond the scope of the present work. In the absence of such data, we conjecture about the variation in orbital domain size as a function of particle size using the existing models[19] of grain growth during grain coarsening/sintering in a solid. The bigger grains grow at the expense of smaller grains during grain growth by two processes: (i) mass transport across the grain boundary, and (ii) grain boundary motion. The grain growth can be slower if the radius ratio (R) between adjacent grains and the overall density of the matrix are below certain critical values.[20] In such a scenario, the grain growth takes place via the mass transport process. The growth can accelerate once these parameters cross the critical values. In that case, the process of grain boundary motion takes over. The anomalous L versus d data, in the present case, can possibly be rationalized by invoking this grain growth scenario. The decrease in particle size could be considered as analogous to sintering/coarsening under pressure. There are, in fact, three different regimes across the entire range of L versus d pattern: between $\sim$100 nm and bulk (I), between $\sim$29 and $\sim$100 nm (II), and finally between $\sim$19 and $\sim$29 nm (III). In regime I, all the orbital domains could be of nearly equal size. They are small with sizable volume fraction of domain boundaries. Therefore, the overall latent heat (L) is small. The growth process is slow as radius ratio between adjacent domains (R) as well as the density of the matrix is low. This process continues till the particle size reaches $\sim$100 nm. In regime II, the growth process accelerates as R and the overall density of the matrix reach the critical values. The domain growth and sintering eventually lead to the formation of single-domain structure near $d \sim 29$ nm. Similar scenario can be observed in packing of granular objects where percolation of force chains gives rise to sharp rise in packing density.[21] Such a clean lattice is normally observed in thin films where one observes sharp improvement in properties compared to those of the bulk system. With further decrease in particle size in regime III, the domain size becomes smaller. Therefore, the latent heat of transition also approaches zero in such a scenario. Such a decrease in domain size could result from two factors: (i) an increase in lattice defects and disorder in finer particles, and (ii) an increase in lattice strain. In fact, over the entire regime of particle sizes, there is always a competition between homogeneous cleaner lattice and strained defective lattice volume fractions. It has been observed from x-ray line profile analysis that lattice strain does increase with the decrease in particle size. So, while the bulk particle contains sizable lattice defects and hence large domain boundaries with smaller domain volume, the particles become essentially defect-free and single-domain ones near an optimum size $d \sim 30$ nm. Even finer particles, of course, contain large defects, twins, as well as disorder, which, in turn, give rise to smaller domains. Such variation in lattice properties could be intrinsic size effect as powders prepared by two different techniques—microemulsion and sonochemical—result in nearly identical results. The plot of L versus orbital domain size, across the bulk to nanoscale particles, is expected to exhibit a monotonically decreasing pattern. This pattern apparently corroborates the results obtained in a series of $La_{1-x}R_xMnO_3$ systems (R=Pr, Nd, Sm, Gd, etc.) where L decreases monotonically with average A-site radius $\langle r_A \rangle$ and thereby with orbital domain size.[22] It is important to point out that in regime III, one does not observe semblance of superpara-orbital-ordered state analogous to superparamagnetic state with no finite T_{JT} and L. Instead, both T_{JT} and L decrease systematically with the decrease in d without dropping to zero abruptly. Direct experimental determination of orbital domain size as a function of particle size will clear the entire scenario and this will be attempted in a future work.

The T_{JT} exhibits a drop with the drop in d. This is primarily because T_{JT} does not depend much on the orbital domain size. Instead, it depends mostly on the average Mn-O-Mn bond angle $\langle \cos^2 \phi \rangle$.[23] In thinner films, it has been found that T_{JT} drops by $\sim$10–20% due to increased lattice strain.[24] T_{JT} also depends on the lattice disorder. Since surface area in nanoparticles increases and, thereby, gives rise to lattice disorder, T_{JT} is found to drop systematically with d. The rise in T_{JT} by a few degrees near $d \approx 30$ nm could result from a competition between increase in surface area and simultaneous decrease in domain boundaries in essentially defect-free bulk regions in a cleaner system. In smaller particles, disorder becomes more as surface area increases rapidly with the drop in particle size. Therefore, T_{JT} is found to decrease again in smaller particle systems. Impact of domain boundaries on T_N is not so prominent and, therefore, T_N depicts no such nonmonotonicity. It decreases monotonically with the

decrease in d, which is quite similar to the decrease in T_N, observed in $R\mathrm{MnO_3}$ with smaller R ions such as Pr, Nd, Sm, etc. due to chemical pressure effect.[23]

The HRTEM data shown in Fig. 2 provide evidence of increased lattice defects in finer particles and seem to support our conjecture of variation in orbital domain size with the decrease in particle size. For example, for the particles of average size ~32 nm, the lattice planes (fringes in the figure), within an isolated particle, are found to be oriented parallel to each other and free from domain boundaries or defects like twinning planes [Fig. 2(a)]. The average lattice plane spacing is ~2.25 Å, which corresponds to the (202) plane. The crystallographic axes are shown corresponding to the HRTEM image. On the other hand, in even finer particle system, the presence of such defect structures within a particle is quite evident. The orientation of the lattice plane changes along defect lines within a small spatial scale. The average lattice spacing for one such set of lattice fringes is ~3.75 Å, which corresponds to the (110) plane. Because of enhanced strain and lattice defects the orbital domain size is expected to be small in finer particles.

In summary, we observe that the latent heat (L) associated with the orbital order-disorder transition in pure $\mathrm{LaMnO_3}$ varies significantly with the average particle size (d). One important observation is almost an order of magnitude rise in L for a particle size $d \sim 30$ nm. Such a large L can be exploited in many applications, if orbital order-disorder transition or melting of orbital order can be driven by photoirradiation or current/magnetic field pulses. The nonmonotonic pattern of variation of L with d could possibly be resulting from nonmonotonic variation of orbital domain size as a function of particle size. Such variation in orbital domain size is possibly due to variation in lattice defects, strain, and disorder. The TEM and HRTEM data provide evidence of increased lattice defects and shell area in core-shell morphology of the particles with the decrease in particle size.

We thank S. Bose of Materials Research Center, Indian Institute of Science, Bangalore, for carrying out the low temperature magnetic measurements and J. Ghosh of CG & CRI for helping in analyzing the x-ray diffraction data. We also thank P. Mandal of the Saha Institute of Nuclear Physics, Calcutta, for providing the single crystal of $\mathrm{LaMnO_3}$.

*Electronic address: dipten@cgcri.res.in

[1] See, for example, Y. Tokura and N. Nagaosa, Science **280**, 462 (2000); D. I. Khomskii, Phys. Scr. **72**, CC8 (2005).
[2] Y. Tokura, Phys. Today **56**(7), 50 (2003).
[3] See, for example, articles in a special issue of New J. Phys. **6**, 152 (2004); see also J. van den Brink, G. Khaliullin, and D. I. Khomskii, in *Colossal Magnetoresistive Manganites*, edited by T. Chatterji (Kluwer, Dordrecht, 2002).
[4] Y. Murakami, J. P. Hill, D. Gibbs, M. Blume, I. Koyama, M. Tanaka, H. Kawata, T. Arima, Y. Tokura, K. Hirota, and Y. Endoh, Phys. Rev. Lett. **81**, 582 (1998); M. v. Zimmermann, C. S. Nelson, Y.-J. Kim, J. P. Hill, D. Gibbs, H. Nakao, Y. Wakabayashi, Y. Murakami, Y. Tokura, Y. Tomioka, T. Arima, C.-C. Kao, D. Casa, C. Venkataraman, and Th. Gog, Phys. Rev. B **64**, 064411 (2001).
[5] C. S. Nelson, J. P. Hill, D. Gibbs, F. Yakhou, F. Livet, Y. Tomioka, T. Kimura, and Y. Tokura, Phys. Rev. B **66**, 134412 (2002).
[6] See, for example, *Nanomaterials: Synthesis, Properties and Applications*, edited by A. S. Edelstein and R. C. Cammarata (Institute of Physics Publishing, Bristol, UK, 1998).
[7] Ph. Buffat and J.-P. Borel, Phys. Rev. A **13**, 2287 (1976).
[8] M. Schmidt, R. Kusche, B. von Issendorff, and H. Haberland, Nature (London) **393**, 238 (1998).
[9] M. Dippel, A. Maier, V. Gimple, H. Wider, W. E. Evenson, R. L. Rasera, and G. Schatz, Phys. Rev. Lett. **87**, 095505 (2001).
[10] M. Zhang, M. Y. Efremov, F. Schiettekatte, E. A. Olson, A. T. Kwan, S. L. Lai, T. Wisleder, J. E. Greene, and L. H. Allen, Phys. Rev. B **62**, 10548 (2000), and references therein.
[11] E. A. Olson, M. Y. Efremov, M. Zhang, Z. Zhang, and L. H. Allen, J. Appl. Phys. **97**, 034304 (2005).
[12] P. Pawlow, Z. Phys. Chem., Stoechiom. Verwandtschaftsl. **65**, 1 (1909); **65**, 545 (1909).
[13] H. Sakai, Surf. Sci. **351**, 285 (1996).
[14] See, for example, P. R. Couchman and W. A. Jesser, Nature (London) **269**, 481 (1977).
[15] X. Wang, J. Zhuang, Q. Peng, and Y. Li, Nature (London) **437**, 121 (2005).
[16] K. Ossero-Asare, in *Handbook of Microemulsion Science and Technology*, edited by P. Kumar and K. L. Mittal (Marcel-Dekker, New York, 1999).
[17] A. Gedanken, Ultrason. Sonochem. **11**, 47 (2004).
[18] See, for example, D. L. Leslie-Pelecky and R. D. Rieke, Chem. Mater. **8**, 1770 (1996).
[19] F. F. Lange and B. J. Kellet, J. Am. Chem. Soc. **72**, 735 (1989), and references therein.
[20] L. C. Chen and F. Spaepen, J. Appl. Phys. **69**, 679 (1991).
[21] H. A. Makse, D. L. Johnson, and L. M. Schwartz, Phys. Rev. Lett. **84**, 4160 (2000).
[22] P. Mondal, D. Bhattacharya, P. Choudhury, P. Mandal, A. N. Das, A. K. Tyagi, and A. K. Raychaudhuri (unpublished); D. Bhattacharya, P. S. Devi, and H. S. Maiti, Phys. Rev. B **70**, 184415 (2004).
[23] J.-S. Zhou and J. B. Goodenough, Phys. Rev. B **68**, 144406 (2003).
[24] J. H. Song, J. H. Park, K.-B. Lee, J. M. Lee, and Y. H. Jeong, Phys. Rev. B **66**, 020407(R) (2002); Q. Qian, T. A. Tyson, C.-C. Kao, W. Prellier, J. Bai, A. Biswas, and R. L. Greene, *ibid.* **63**, 224424 (2001).